

# The extended ROSAT-ESO Flux Limited X-ray Galaxy Cluster Survey (REFLEX II)

## IV. X-ray Luminosity Function and First Constraints on Cosmological Parameters <sup>★</sup>

Hans Böhringer<sup>1</sup>, Gayoung Chon<sup>1</sup>, Chris A. Collins<sup>2</sup>

<sup>1</sup> Max-Planck-Institut für extraterrestrische Physik, D-85748 Garching, Germany.

<sup>2</sup> Astrophysics Research Institute, Liverpool John Moores University, IC2, Liverpool Science Park, 146 Brownlow Hill, Liverpool L3 5RF, UK

Submitted 29/11/13

### ABSTRACT

The X-ray luminosity function which is closely related to the cluster mass function is an important statistic of the census of galaxy clusters in our Universe. It is also an important means to probe the cosmological model of our Universe. Based on our recently completed REFLEX II cluster sample comprising 910 galaxy clusters with redshifts we construct the X-ray luminosity function of galaxy clusters for the nearby Universe and discuss its implications. We derive the X-ray luminosity function of the REFLEX II clusters on the basis of a precisely constructed selection function for the full sample and for several redshift slices from  $z = 0$  to  $z = 0.4$ . In this redshift interval we find no significant signature of redshift evolution of the luminosity function. We provide the results of fits of a parameterized Schechter function and extensions of it which provide a reasonable characterization of the data. We also use a model for structure formation and galaxy cluster evolution to compare the observed X-ray luminosity function with the theoretical predictions for different cosmological models. The most interesting constraints can be derived for the cosmological parameters  $\Omega_m$  and  $\sigma_8$ . We explore the influence of several model assumptions on which our analysis is based. We find that the scaling relation of X-ray luminosity and mass introduces the largest systematic uncertainty. From the statistical uncertainty alone we can constrain the matter density parameter,  $\Omega_m \sim 0.27 \pm 0.03$  and the amplitude parameter of the matter density fluctuations,  $\sigma_8 \sim 0.80 \pm 0.03$ . Marginalizing over the most important uncertainties, the normalisation and slope of the  $L_X - M$  scaling relation, we have larger error bars and a result of  $\Omega_m \sim 0.29 \pm 0.04$  and  $\sigma_8 \sim 0.77 \pm 0.07$  ( $1\sigma$  confidence limits). We compare our results with those of the SZ-cluster survey provided by the PLANCK mission and we find very good agreement with the results using PLANCK clusters as cosmological probes, but we have some tension with PLANCK cosmological results from the microwave background anisotropies, which we discuss in the paper. We also make a comparison with results from the SDSS cluster survey, several cosmological X-ray cluster surveys, and recent Sunyaev-Zel'dovich effect surveys. We find good agreement with these previous results and show that the REFLEX II survey provides a significant reduction in the uncertainties compared to earlier measurements.

**Key words.** X-rays: galaxies: clusters, Galaxies: clusters: Intergalactic medium, Cosmology: observations

### 1. Introduction

Galaxy clusters as the largest, clearly defined objects in our Universe are interesting astrophysical laboratories and important cosmological probes (e.g. Sarazin 1986, Borgani et al. 2001, Voit 2005, Vikhlinin et al. 2009, Allen et al. 2011, Böhringer 2011). They are particularly good tracers of the large-scale structure of the cosmic matter distribution and its growth with time. While most of the precise knowledge on the galaxy cluster population has come from X-ray observations as detailed in the above references, recent progress has also been made by optical cluster surveys (e.g. Rozo et al. 2010) and millimeter wave surveys using the Sunyaev-Zel'dovich effect (Reichardt et al. 2012, Benson et al. 2013, Marriage et al. 2011, Sehgal et al. 2011, PLANCK-Collaboration 2011, 2013b). X-ray surveys for galaxy clusters are still most advanced providing statistically well defined, approximately mass selected cluster samples, since: (i) X-ray lumi-

osity is tightly correlated to mass (e.g. Reiprich & Böhringer 2002, Pratt et al. 2009), (ii) bright X-ray emission is only observed for evolved clusters with deep gravitational potentials, (iii) the X-ray emission is highly peaked and projection effects are minimized, and (iv) for all these reasons the survey selection function can be accurately modeled.

The ROSAT All-Sky Survey (RASS, Trümper 1993) is the only existing full sky survey conducted with an imaging X-ray telescope, providing a sky atlas in which one can search systematically for clusters in the nearby Universe. The largest, high-quality sample of X-ray selected galaxy clusters is provided so far by the REFLEX Cluster Survey (Böhringer et al. 2001, 2004, 2013) based on the southern extragalactic sky of RASS at declination  $\leq 2.5$  degree. The quality of the sample has been demonstrated by showing that it can provide reliable measures of the large-scale structure (Collins et al. 2000, Schuecker et al. 2001a, Kerscher et al. 2001), yielding cosmological parameters (Schuecker et al. 2003a, b; Böhringer 2011) in good agreement within the measurement uncertainties with the subsequently published WMAP results (Spergel et al. 2003, Komatsu

Send offprint requests to: H. Böhringer, hxb@mpe.mpg.de

<sup>★</sup> Based on observations at the European Southern Observatory La Silla, Chile

et al. 2011). The REFLEX data have also been used to study the X-ray luminosity function of galaxy clusters (Böhringer et al. 2002), the galaxy velocity dispersion - X-ray luminosity relation (Ortiz-Gil et al., 2004), the statistics of Minkowski functionals in the cluster distribution (Kerscher et al. 2001), and to select statistically well defined subsamples like the HIFLUGCS (Reiprich & Böhringer 2002) and REXCESS (Böhringer et al. 2007). The latter is particularly important as a representative sample of X-ray surveys to establish X-ray scaling relations (Croston et al. 2008, Pratt et al. 2009, 2010, Arnaud et al. 2010) and the statistics of the morphological distribution of galaxy clusters in X-rays (Böhringer et al. 2010).

Recently we have completed an extension of REFLEX apart from 11 missing redshifts, REFLEX II, which about doubles the size of the cluster sample. The construction of this sample is described in Böhringer et al. (2013). In the present paper we describe the construction of the REFLEX II X-ray luminosity function from the galaxy cluster data and the survey selection function derived in Böhringer et al. (2013). We fit parameterized functions to the data and we compare the observed luminosity function to the predictions of cosmological structure formation models. From the latter comparison we obtain constraints on cosmological parameters. The most sensitive of these parameters are the matter density parameter,  $\Omega_m$ , and the amplitude parameter of the matter density fluctuations,  $\sigma_8$ . We focus on the derivation of robust constraints on the two parameters in this paper, while leaving a comprehensive modeling of the combined uncertainty of all relevant cosmological and cluster parameters to a future publication. We study the errors introduced by various other uncertainties rather case by case and evaluate the overall systematic errors. The REFLEX II cluster sample has also recently been used to construct the first supercluster catalog for clusters with a well defined selection function (Chon & Böhringer 2013), showing among other results that the X-ray luminosity function of clusters in superclusters is top-heavy in comparison to that of clusters in the field.

A preliminary sample of REFLEX II which had 49 redshifts less than used here, has been applied to the study of the galaxy cluster power spectrum by Balaguera-Antolinez et al. (2011). The results show a very good agreement with the cosmological predictions based on cosmological parameters determined from WMAP 5 yr data. In a second paper (Balaguera-Antolinez et al. 2012), in which the construction of REFLEX mock samples from simulations used in the earlier paper is described, a preliminary X-ray luminosity function of REFLEX II has been determined. Here we use a completely new approach with updates on the cluster sample, the scaling relations, and the missing flux correction used in the sample construction, and the survey selection function based on the procedures described in Böhringer et al. (2013).

Other previous determinations of the X-ray luminosity function of galaxy clusters include: Piccinotti et al. (1982), Kowalski et al. (1984), Gioia et al. (1984), Edge et al. (1990), Henry et al. (1992), Burns et al. (1996), Ebeling et al. (1997), Collins et al. (1997), Burke et al. (1997), Rosati et al. (1998), Vikhlinin et al. (1998), De Grandi et al. (1999), Ledlow et al. (1999), Nichol et al. (1999), Gioia et al. (2001), Donahue et al. (2001) Allen et al. (2003), Mullis et al. (2004), Böhringer et al. (2007), Koens et al. (2013).

The paper is organized as follows. In chapter 2 we introduce the REFLEX II galaxy cluster sample and the survey selection function. In section 3 we use the parameterized Schechter function fitted to our data to describe the resulting X-ray luminosity function. In section 4 we outline the cosmological modeling used

for the theoretical prediction of the cluster mass and X-ray luminosity function. In section 5 we discuss the results of the model comparison to the data for different cosmological models. The effect of the uncertainties in the used cluster scaling relations on the results is discussed in section 6 and other systematic uncertainties of our analysis are discussed in section 7. In section 8 we compare our results to findings from other surveys and section 9 closes the paper with the summary and conclusions.

If not stated otherwise, we use for the calculation of physical parameters and survey volumes a geometrically flat  $\Lambda$ -cosmological model with  $\Omega_m = 0.3$  and  $h_{70} = H_0/70 \text{ km s}^{-1} \text{ Mpc}^{-1} = 0.7$ . All uncertainties without further specifications refer to  $1\sigma$  confidence limits.

## 2. The REFLEX II Galaxy Cluster Survey

The REFLEX II galaxy cluster survey is based on the detection of galaxy clusters in the RASS (Voges et al. 1999). The region of the survey is the southern sky below equatorial latitude  $+2.5 \text{ deg.}$  at galactic latitude  $b_{II} \geq 20 \text{ deg.}$  The regions of the Magellanic clouds have been masked. The survey region selection, the source detection, the galaxy cluster sample definition and compilation, and the construction of the survey selection function as well as tests of the completeness of the survey are described in Böhringer et al. (2013). In brief the survey area is  $\sim 2.4 \text{ ster}$  or 13924 square degrees. The nominal flux limit down to which galaxy clusters have been identified in the RASS in this region is  $1.8 \times 10^{-12} \text{ erg s}^{-1} \text{ cm}^{-2}$  in the 0.1 - 2.4 keV energy band. For the construction of the X-ray luminosity function in this paper we impose an additional cut on the minimum number of detected source photons of 20 counts. This has the effect that the nominal flux cut quoted above is only reached in about 80% of the survey and in regions with lower exposure and higher interstellar absorption the flux limit is accordingly higher (see Fig. 11 in Böhringer et al. 2013). This effect is modeled and taken into account in the survey selection function.

The flux limit imposed on the survey is for a nominal flux, that has been calculated from the detected photon count rate for a cluster X-ray spectrum characterized by a temperature of 5 keV, a metallicity of 0.3 solar, a redshift of zero, and an interstellar absorption column density given by the 21cm sky survey described by Dickey and Lockmann (1990). This count rate to flux conversion is appropriate prior to any redshift information and is analogous to an observed object magnitude corrected for galactic extinction in the optical.

After the redshifts have been measured, a new flux is calculated taking the redshifted spectrum and an estimate for the spectral temperature into account. The temperature estimate is obtained from the X-ray luminosity - temperature relation of Pratt et al. (2009) determined from the REXCESS cluster sample, which is a sample of clusters drawn from REFLEX I for deeper follow-up observations with XMM-Newton and which is representative of the entire flux limited survey (Böhringer et al. 2007). The luminosity is determined first from the observed flux by means of the luminosity distance for a given redshift. Using the X-ray luminosity mass relation given in Pratt et al. (2009) we can then use the mass estimate to determine a fiducial radius of the cluster, which is taken to be  $r_{500}^1$ . We then use a beta model for the cluster surface brightness distribution to correct for the possibly missing flux in the region between the detection aper-

<sup>1</sup>  $r_{500}$  is the radius where the average mass density inside reaches a value of 500 times the critical density of the Universe at the epoch of observation.

ture of the source photons and the radius  $r_{500}$ . The procedure to determine the flux, the luminosity, the temperature estimate, and  $r_{500}$  is done iteratively and described in detail in Böhringer et al. (2013). In that paper we deduced a mean flux uncertainty for the REFLEX II clusters of 20.6%, which is mostly due to the Poisson statistics of the source counts but also contains some systematic errors. In this paper we will for the following analysis adopt a flux and luminosity measurement uncertainty of 20%.

The X-ray source detection and selection is based on the official RASS source catalogue by Voges et al. (1999). We have been using the publically available final source catalog<sup>2</sup> as well as a preliminary source list that was created in the course of the production of the public catalog. The latter source list had a lower significance limit and included a larger number of detections, but it had not been manually screened as the public data set. This ensured a higher completeness of the input catalog and spurious sources are caught by our subsequent screening. Since the analysis software used to produce the public RASS source catalog is tuned for point sources and does not perform so well for the extended sources of galaxy clusters, we have reanalyzed all the X-ray sources with the growth curve analysis method (Böhringer et al. 2000). The flux cut was imposed on the reanalysed data set. The results of the flux determination was inspected visually for all sources above and near the flux limit and pathological cases as well as cases of source confusion have been corrected manually.

The galaxy clusters among the sources have been identified using all available means: X-ray source properties, available optical images (mostly from DSS<sup>3</sup>), literature data (mostly from NED<sup>4</sup>) and finally by follow-up observations at ESO La Silla. The source identification scheme is described in detail in Böhringer et al. (2013). The redshifts have been secured mostly by multi-object spectroscopy and the redshift accuracy of the clusters is typically 60 km/s (Guzzo et al. 2009, Chon & Böhringer 2012).

The survey selection function is a very important survey product that is crucial for the work of this paper. We have constructed the selection function in the form of a survey mask that provides the limiting X-ray luminosity for the cluster detection as a function of the sky position and redshift. For the sky position the survey mask is currently given in pixels of one square degree. The survey mask takes all the systematics of the RASS exposure distribution, galactic absorption, the fiducial flux, the detection count limit, and all the applied corrections described above into account. The survey mask is given in three dimensional form so that it can also be used for any study that is related to the spatial distribution of the clusters. A preliminary version of it has been used for the construction of the cluster density distribution power spectrum and a preliminary construction of the luminosity function in Balaguera-Antolinez et al. (2011, 2012). It allows further to select a cluster sample from simulations in a precisely analogous way as the REFLEX II survey selects the clusters from the sky.

The survey selection function provides the means to calculate the effective survey volume as a function of the X-ray luminosity. This survey volume function is shown in Fig. 1 for different imposed redshift limits. The objects with the lowest X-ray

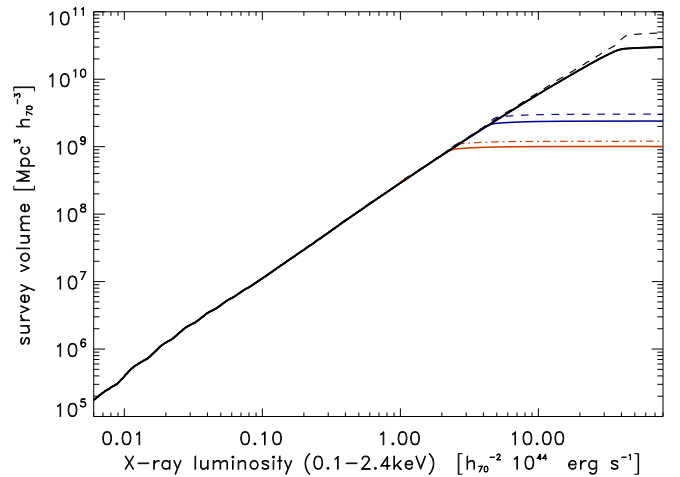


**Fig. 1.** Effective survey volume as a function of X-ray luminosity. The survey volume has been calculated for three different cut-off redshift,  $z = 0.8$ ,  $z = 0.3$ ,  $z = 0.22$  for our reference cosmology ( $h = 0.7$ ,  $\Omega_m = 0.3$  and  $\Omega_\Lambda = 0.7$ ). We have also determined the same set of curves for a cosmology with the parameters  $h = 0.7$ ,  $\Omega_m = 0.26$  and  $\Omega_\Lambda = 0.74$  shown as dashed curves. **Note** that the difference between the set of curves has been amplified by a factor of 10, to make the offset better visible. This affects the dashed curves which are shown slightly offset from the original position.

luminosities are only detected in a small volume in the nearby Universe due to the flux limit of the survey. The luminous clusters with  $L_X \geq 2.5 \times 10^{44} \text{ erg s}^{-1}$  are found in a volume larger than  $1 \text{ Gpc}^3$ . We also show the survey volume calculated for two different cosmological models in the Figure including the reference cosmology used in the paper ( $h = 0.7$ ,  $\Omega_m = 0.3$  and  $\Omega_\Lambda = 0.7$ ) and a cosmology closer the WMAP results (Komatsu et al. 2011) with parameter values of  $h = 0.7$ ,  $\Omega_m = 0.26$  and  $\Omega_\Lambda = 0.74$ . The difference is rather small and we have exaggerated the difference between the curves representing the two cosmologies by a factor of 10 to make it better visible. The largest difference is found for the survey volume at the cut-off redshift, since at lower redshifts the effect of the cosmological model on the deduced luminosity and survey volume partly compensate to produce very similar curves.

In the following we will use different versions of these calculations, to also determine the selection function in redshift shells. For the proper cosmological modeling of the results we determine the survey volume for any given cosmology used in the model fitting process.

### 3. The X-ray luminosity function

The X-ray luminosity function (XLF) is determined from the catalog of clusters and the survey selection function in the form of the effective survey volume as a function of X-ray luminosity as shown in Fig. 1. We use a source detection count cut of minimum 20 photons for the selection. Then the binned differential X-ray luminosity function is given by

$$\frac{dn(L_X)}{dL_X} = \frac{1}{\Delta L_X} \sum_i \frac{1}{V_{max}(L_{X_i})} \quad (1)$$

where  $V_{max}$  is the effective detection volume and  $\Delta L_X$  is the width of the luminosity bin and the sum includes all clusters

<sup>2</sup> the RASS source catalogs can be found at: <http://www.xray.mpe.mpg.de/rosat/survey/rass-bsc/> for the bright sources and <http://www.xray.mpe.mpg.de/rosat/survey/rass-fsc/> for the faint sources

<sup>3</sup> see <http://archive.stsci.edu/dss/>

<sup>4</sup> see <http://ned.ipac.caltech.edu/>

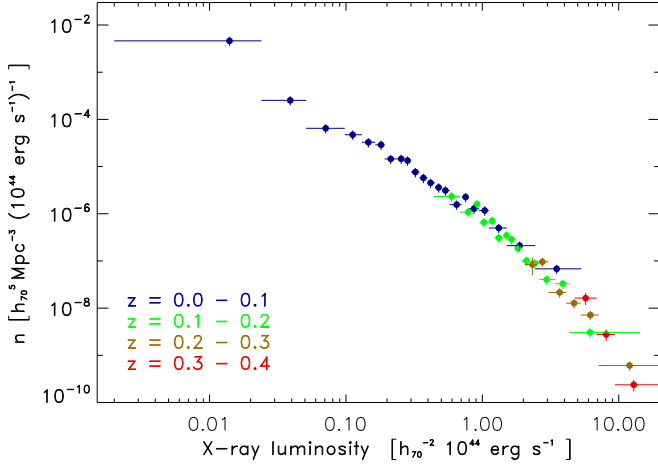


**Fig. 2.** X-ray luminosity function of REFLEX II determined in four equidistant redshift shells from  $z = 0$  to  $z = 0.4$ . Due to the flux limit of the sample the different redshift shells cover different luminosity ranges. In the overlap region the functions show no major differences.

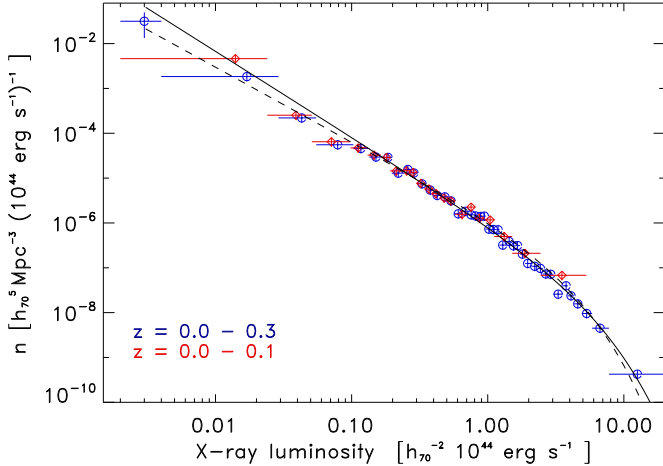


**Fig. 3.** X-ray luminosity function of the REFLEX II galaxy cluster survey averaged over the survey volumes out to redshift  $z = 0.1$  and  $z = 0.3$ . Schechter functions have been fit to the two data sets separately to visualize the potential difference of the functions. The fits were performed over the whole observed X-ray luminosity range.

in the bin. Figs. 2 and 3 show the XLF derived for a binning with 20 clusters per bin, except for the bin at the lowest X-ray luminosity, for different redshift ranges. While Fig. 2 presents the XLF in four equidistant redshift shells from  $z = 0$  to  $z = 0.4$ ,

The luminosity values used in the construction of the XLF are the luminosities inside  $r_{500}$ , corrected for missing flux in the 0.1 - 2.4 keV rest frame band. The errors for the XLF given in the Figures are the Poisson uncertainties for the number of clusters per bin.

Looking for evolutionary effects in the XLF in Fig. 2, we do not detect any significant difference of the functions, which implies no severe deficiencies in the cluster detection in the high redshift shells and no strong evolutionary effects. What is expected from theory is mostly a change at the high luminosity end, where the lower redshift shells should show more luminous

clusters than the more distant ones. In Appendix A we show the expectation for our best fitting cosmological model. While the mass function would show a more noticeable change with redshift, the corresponding change in the XLF is small as the evolution effect is partly compensated by the adopted redshift evolution of the X-ray luminosity - mass relation. In the theoretical functions we see a significant difference only at luminosities above about  $6 \times 10^{44} h_{70}^{-2} \text{ erg s}^{-1}$  where we have hardly any objects and no statistics in the two lowest redshift shells below  $z = 0.2$ .

Fig. 3 compares the XLF in the two redshift ranges from  $z = 0$  to  $z_{max} = 0.1$  and  $z_{max} = 0.3$ , respectively. There are 419 clusters at  $z < 0.1$  and 802 clusters at  $z < 0.3$  for  $L_X \geq 3 \times 10^{42} \text{ erg s}^{-1}$ . In the larger volume at  $z > 0.3$  there are 53 additional clusters. Constructing the XLF in an even larger volume (e.g. for  $z_{max} = 0.8$ ) shows hardly any difference in the resulting function. To make it even more clear that there is not much leverage to look for redshift evolution in the data, we fit Schechter functions to the two data sets (as will be explained in the next section), which are also shown in the Figure. The Schechter fit prefers a slightly less top-heavy luminosity function for the lowest redshift bin. We will therefore not further pursue a detailed modeling of the evolution of the XLF in this paper and assume that the XLF can be described reasonably well by a constant function in the redshift range  $z = 0 - 0.4$ .

### 3.1. Fits of a Schechter function

For an analytical, phenomenological description of the REFLEX X-ray luminosity function we fit a Schechter function of the form

$$n(L_X) dL_X = n_0 \left( \frac{L_X}{L_X^*} \right)^{-\alpha} \exp\left(-\frac{L_X}{L_X^*}\right) \frac{dL_X}{L_X^*} \quad (2)$$

to the data.

We use a maximum likelihood method to determine the best fitting Schechter function parameters by comparing the predicted and observed X-ray luminosity distribution of the galaxy clusters. The approach we take is similar to what we used in Schuecker & Böhringer (1998) and Böhringer et al. (2002; see also Daley & Vere-Jones 1988 and for a similar application Marshall et al. 1983 and Henry 2004). To test a distribution function,  $\lambda(x)$ , with discrete observational data points,  $\lambda(x_i)$ , we minimize the likelihood function:

$$\ln L = - \int \lambda(x) dx + \sum_{i=1}^N \ln \lambda(x_i) \quad (3)$$

The distribution function  $\lambda(x)$  should describe observables. In our case we compare the observed and predicted X-ray luminosity distribution of the clusters. The X-ray luminosities can be considered to be almost direct observables, as the spectral model assumptions used for their derivation are safe and possible changes have very small influence on the resulting luminosities. Before the comparison, the predicted X-ray luminosity distribution,  $N(L_X)$ , is folded with the observational error in the following way:

$$N(L_X) = \int_{L_{Xmin}}^{\infty} n(L'_X) V_{max}(L'_X) \Psi(L'_X, L_X) dL'_X \quad (4)$$

where  $n(L'_X)$  is the Schechter luminosity function and  $\Psi(L'_X, L_X)$  represents the Gaussian error distribution for the mean measurement uncertainty of 20%.

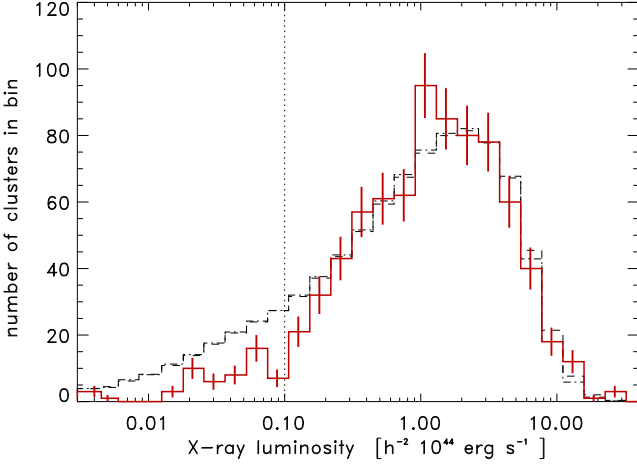


**Fig. 4.** X-ray luminosity histogram of the REFLEX II clusters at  $z \leq 0.3$  (red line with error bars) compared to the best fitting Schechter function for the X-ray luminosity range  $L_X \geq 0.1 \times 10^{44} \text{ erg s}^{-1}$ . The X-ray luminosity limit is indicated by the vertical dotted line. The error bars give the Poisson uncertainty of the counts in the bins.

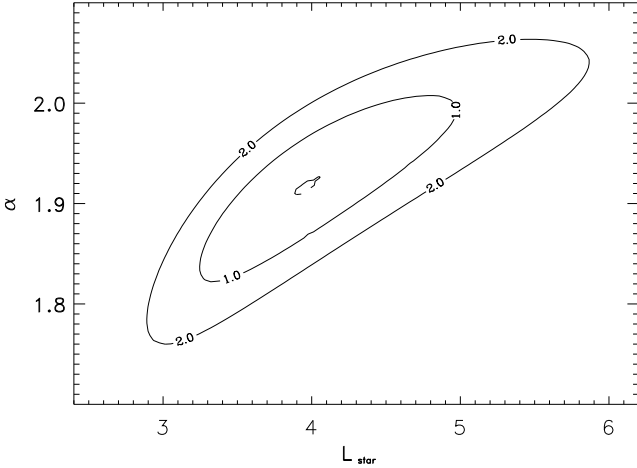


**Fig. 5.** Constraints on the Schechter parameters  $\alpha$  and  $L_X^*$  from the fit to the data of the X-ray luminosity function of REFLEX II for  $z \leq 0.3$  and luminosity range  $L_X \geq 0.1 \times 10^{44} \text{ erg s}^{-1}$ .

Fig. 4 shows the luminosity distribution function and the fit for the redshift range  $z \leq 0.3$  and the luminosity range  $L_X \geq 10^{43} \text{ erg s}^{-1}$ . The uncertainties of the fit for the two most important parameters,  $\alpha$  and  $L_X^*$  are shown in Fig. 5, where we give the 1 and  $2\sigma$  constraints. The typical  $1\sigma$  uncertainties – similar for fits in different X-ray luminosity ranges – are  $\Delta\alpha = 5\%$  and  $\Delta L_X^* = 22\%$ .

The X-ray luminosity function is now observationally so well constrained, that a Schechter fit is not any more an adequate description. Studying the fits for varying X-ray luminosity ranges as shown in Table 1, we note that fits limited to the higher luminosity side of the luminosity function require a steeper slope, and the fit is forced to a shallower slope for the full range of X-ray luminosities, at the expense of a worse fit in the high and intermediate luminosity range.

**Table 1.** Best fitting parameters for a Schechter function and alternative functions to the REFLEX II X-ray luminosity function.

method	$L_x$ – range	$\alpha$	$L_X^*$	$n_0$	$q$	$\eta$	no.cl.
A	$\geq 0.003$	1.74	3.02	$5.0 \cdot 10^{-7}$	–	2.3	802
A	$\geq 0.01$	1.76	3.10	$4.7 \cdot 10^{-7}$	–	2.5	798
A	$\geq 0.03$	1.78	3.19	$4.5 \cdot 10^{-7}$	–	2.9	779
A	$\geq 0.1$	1.93	3.99	$2.8 \cdot 10^{-7}$	–	9.9	741
A	$\geq 0.3$	2.03	4.67	$2.0 \cdot 10^{-7}$	–	24.3	623
B	$\geq 0.003$	1.54	1.08	$1.8 \cdot 10^{-6}$	1.39	1.4	802
B	$\geq 0.01$	1.53	1.03	$2.0 \cdot 10^{-6}$	1.39	1.4	802
B	$\geq 0.1$	1.60	1.17	$1.6 \cdot 10^{-6}$	1.39	2.5	802
C	$\geq 0.003$	2.19	5.7	$1.3 \cdot 10^{-7}$	–	1.6	802
C	$\geq 0.01$	2.18	5.5	$1.4 \cdot 10^{-7}$	–	1.6	798
C	$\geq 0.03$	2.13	5.0	$1.7 \cdot 10^{-7}$	–	1.4	779
C	$\geq 0.1$	2.18	5.4	$1.4 \cdot 10^{-7}$	–	1.7	741
C	$\geq 0.3$	2.17	5.4	$1.4 \cdot 10^{-7}$	–	1.6	623

**Notes:** The method code A is for the Schechter function (Eq. 2), B for the q-exponential (Eq. 5) and C for the modified Schechter function (Eq. 6). The X-ray luminosity range used in the fit and the parameter  $L_X^*$  are given in units of  $10^{44} h_{70}^{-2} \text{ erg s}^{-2}$ .  $\alpha$ ,  $L_X^*$ , and  $n_0$  (in units of  $h_{70}^3 \text{ Mpc}^{-3}$ ) are the slope, the break parameter and the normalisation of the Schechter function or its modified variants, while  $q$  is the extra parameter of the q-exponential function.  $\eta$  is similar to a reduced  $\chi^2$  parameter determined as explained in the text and the last column gives the number of clusters involved in the fit. The typical uncertainties are  $\sim 5\%$  for  $\alpha$  and  $\sim 22\%$  for  $L_X$ .

### 3.2. Alternative fitting functions

Since the Schechter function does not provide such a satisfying analytical description of the REFLEX II X-ray luminosity function, we have also tried alternative functions for the fit. As already used in our previous paper by Balaguera-Antolinez (2012) we apply a q-exponential function of the following form:

$$n(L_X) dL_X = n_0 \left( \frac{L_X}{L_X^*} \right)^{-\alpha} \left[ 1 + \frac{L_X}{L_X^*} (1-q) \right]^{\frac{1}{1-q}} \frac{dL_X}{L_X} \quad (5)$$

The effect of the q-exponential function is to cause a sharper decrease of the Schechter function at high luminosities. This extra degree of freedom helps to improve the fit as can be seen in Table 1.

To estimate how good the fit reproduces the data we calculate the squared difference of the observed number of clusters in luminosity bins compared to the predicted using Eqs. 2, 5, and 6 normalized by the Poisson error of the observations. We derive a parameter denoted  $\eta$  which is the sum of the squared normalized differences over all bins, divided by the number of bins. This is very similar to a reduced  $\chi^2$ , with the difference that we do not normalize by the degrees of freedom. We prefer to use the parameter  $\eta$  since we want to characterize the deviation from the data rather than the statistical significance of the fit. The summation is carried out only over those bins with either a detection of at least one cluster or a predicted number larger than 0.1. The values are given in Table 1. While the fit is performed using data in the given luminosity range, the  $\eta$  parameter is always given for the full luminosity range. One clearly notes the improvement of the fit for the q-exponential function. Comparing the fit for the q-exponential function with the earlier fitting results of Balaguera-Antolinez (2011), which are converted to our cosmology model

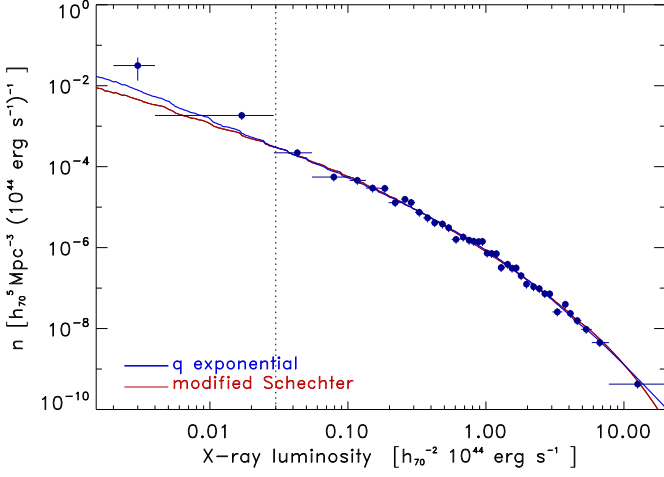


**Fig. 6.** X-ray luminosity function of REFLEX II for a redshift limit of  $z = 0.3$  fitted by a q-exponential function and by the modified Schechter function. Both fits were performed for the X-ray luminosity range  $L_X \geq 0.03 \times 10^{44} \text{ erg s}^{-1}$  indicated by the vertical dotted line.

as  $\alpha = 1.54$ ,  $L_X^* = 1.2 \times 10^{44} h_{70}^{-2} \text{ erg s}^{-1}$ ,  $n_0 = 1.4 \times 10^{-6} h_{70}^3 \text{ Mpc}^{-3}$ , and  $q = 1.3$ , we find a good agreement given the fact that the sample was completed with additional cluster redshifts and the scaling relations used were slightly improved.

Probably an even better way to arrive at a stable fit is to decrease the slope of the fitting function towards low luminosities. For this reason we also tried another modification of the Schechter function which bends the function down at very low luminosities. This modified function has the form:

$$n(L_X) dL_X = n_0 \left( \frac{L_X}{L_X^*} \right)^{-\alpha} \exp\left(-\frac{L_X}{L_X^*}\right) \left[ 1 - \left( 1 + \frac{L_X}{\beta} \right)^{-\gamma} \right] \frac{dL_X}{L_X^*} \quad (6)$$

where  $\beta = 0.25$  and  $\gamma = 1.7$  are extra parameters. Rather than determining these two extra parameters in an overall fit, we found suitable parameters before the final fit. This keeps the number of fit parameters small, avoids degeneracies, and thus allows for a better comparison of the different fitting results.

We note that the fits are more stable and we basically recover a good fitting function for the whole luminosity range even if the fit is restricted to  $L_X \geq 0.3 \times 10^{44} \text{ erg s}^{-1}$ . Therefore we consider the fitting results of this function as our best description, at least for the luminosity range  $L_X \geq 0.02 \times 10^{44} \text{ erg s}^{-1}$ . The fits for the q-exponential and the modified Schechter function are shown in Fig. 6. The fits do not very well describe the first two data points which lay outside the fitted range, but note that these bins only contain 23 clusters together and we put most emphasis on a good fit for the rest of the data.

### 3.3. Comparison to previous determinations of the X-ray luminosity function

Previously determined XLF at low redshift generally show good agreement with the REFLEX I XLF within the error limits of these smaller cluster samples. This includes in particular the low redshift part of the RDCS, 400 deg<sup>2</sup>, and WARPS surveys (Rosati et al. 2002, Mullis et al. 2004, and Koens et al. 2013) and further references therein. The REFLEX I survey is in good agreement with the present results. The Schechter function fit presented for REFLEX I in Böhlinger et al. (2002) is close to the

present fit in the luminosity range  $L_X \geq 3 \times 10^{42} \text{ erg s}^{-1}$ . The small difference is that the REFLEX I function is slightly lower at small values of  $L_X$ , which is due to a better sampling of the poor groups in REFLEX II, and REFLEX I slightly overshoots at high values of  $L_X$  which is mostly due to a small decrease in the scaling radius for massive clusters with the new scaling relations. These small changes do not affect the agreement with previous results for the XLF.

## 4. Model predictions of the cluster X-ray luminosity function

The XLF of galaxy clusters can be used to obtain constraints on cosmological model parameters, notably on the matter density parameter  $\Omega_m$  and the amplitude parameter of the dark matter density fluctuations,  $\sigma_8$ . For the determination of these parameters we need to compare the prediction of the XLF for specific cosmological models with our observations. In this section we describe our method for this prediction.

In the first step of the calculations we determine the cluster mass function based on the recipe given by Tinker et al. (2008). A prerequisite for this calculation is the specification of the statistics of the large-scale structure in the form of the dark matter density fluctuation power spectrum. For the shape of the power spectrum we assume that the initial power spectrum in the early Universe is described by a power law with slope of 0.96 (consistent with the latest result from the Planck Mission (Planck Collaboration 2013b)). We model the structure evolution to the present epoch by a transfer function as given by Eisenstein & Hu (1998) including baryonic acoustic oscillations for a baryon density of  $\Omega_b = 0.045$ . The amplitude of the power spectrum is specified by the amplitude parameter,  $\sigma_8$ . This parameter is the variance of the fluctuation field filtered with a top-hat filter, as shown in Eq. 7 below, with a radius of  $8h^{-1} \text{ Mpc}$ . For the formula of the mass function we calculate the variance of the filtered field through

$$\sigma^2(R_F) = \frac{1}{2\pi^2} \int P(k) \tilde{W}_{TH}^2(R_F, k) k^2 dk \quad (7)$$

where  $P(k)$  is the power spectrum at the epoch of consideration,  $\tilde{W}_{TH}(R_F, k)$  is the top hat filter in Fourier space with filter radius  $R_F$  in real space, and  $\sigma(R_F)^2$  is the variance of the density fluctuation field. The variance as a function of filter radius can be transformed into a function of mass, using the mean density of the Universe,  $\bar{\rho}_m$ . The filter mass is given by  $M = \frac{4\pi}{3} \bar{\rho}_m R_F^3$  and the mass function can then be written by

$$\frac{dn}{dM} = f[\sigma(M)] \frac{\bar{\rho}_m}{M} \frac{d \ln \sigma^{-1}}{dM} \quad (8)$$

with

$$f[\sigma(M)] = A \left[ \left( \frac{\sigma}{b} \right)^{-a} + 1 \right] \exp\left(\frac{c}{\sigma^2}\right) \quad (9)$$

Here  $M$  is the mass of the dark matter halos or clusters in terms of an overdensity of 180 over the mean density of the Universe,  $\bar{\rho}_m$ . We use for the overdensity the value of 180 and the following values for the open parameters in Eq. 9,  $A = 0.186$ ,  $a = 1.47$ ,  $b = 2.57$ , and  $c = 1.19$  as given in Table 2 of Tinker et al. (2008). Some of these parameters are assumed to have a redshift dependence. We use the following parametrizations,  $A(z) = A_0(1+z)^{-0.14}$ ,  $a(z) = a_0(1+z)^{-0.06}$ , and  $b(z) = b_0(1+z)^{-\alpha}$  with  $\log \alpha = \left[ \frac{0.75}{\log(\Delta/75)} \right]^{1.2}$ .

The mass given by this equation is the mass inside a mean overdensity of 180 above the mean density of the Universe. We will be using masses defined for a mean overdensity of 200 above the critical density of the Universe at the epoch of light emission of the observed object. Therefore we have to transform the mass equation into our definition. For the conversion we assume that the mass profile of all clusters can be described by a NFW-model profile (Navarro, Frenk & White 1995, 1997) with a concentration parameter of 5.

Note that we will be using the following conventions throughout the paper. We will use an overdensity of 200 over the critical density of the Universe to characterize the mass of the clusters (which is actually an intermediate parameter not essential for the final results), because this mass is closer to what we usually understand as the virial mass. The X-ray parameters, like the X-ray luminosity are given inside a radius of  $r_{500}$ , because this is closer to the observed aperture in which X-ray luminosity is observationally determined. We do not introduce an inconsistency by using different fiducial radii for mass and luminosity as long as we have a careful book-keeping of all the conversions and scaling relations.

We then use an empirical mass - X-ray luminosity scaling relation of the form

$$L_{500}(0.1 - 2.4 \text{ keV}) = 0.1175 M_{200}^{\alpha_{sl}} h^{\alpha_{sl}-2} E(z)^{\alpha_{sl}} \quad (10)$$

where  $\alpha_{sl}$  is the slope of the scaling relation and  $E(z) = H(z)/H_0$  is the evolution parameter related to the Hubble constant. The unit for  $L_{500}$  is  $10^{44} h_{70}^{-2} \text{ erg s}^{-1}$  (0.1 - 2.4 keV) and for  $M_{200}$  it is  $10^{14} h_{70}^{-1} M_{\odot}$ . The redshift evolution of this relation is based on the assumption of no evolution of the  $L_X - T$  relation. For a discussion of this choice see Böhringer et al. (2012). We also take into account that this relation has an intrinsic scatter with a preferred value of  $\log \sigma_{L_X} = 0.114$  which corresponds to about 30%. We further fold in an observational error of the luminosity of 20% which is the fractional mean error in the flux determination of the REFLEX II cluster sample (Böhringer et al. 2013).

For the slope of the  $L_X - M$  scaling relation,  $\alpha_{sl}$ , we explore two values, 1.51 and 1.61 to illustrate our uncertain knowledge. The value of 1.61 is motivated by the results of our REXCESS study (Pratt et al. 2009) and the analysis of Vikhlinin et al. (2009). For REXCESS a lower value of 1.53 is obtained before the assumed Malmquist bias correction. In comparison to several other studies these values for the slope are on the high side (see our survey of the topic in Böhringer et al. 2012). For example the complete HIFLUGCS sample of 63 clusters gives a value of 1.46, the extended HIFLUGCS a value of 1.61 (Reiprich & Böhringer 2002). Maughan (2007) finds 1.45 in their cosmological analysis. Mantz et al. (2008) find a best fitting value of 1.24. Therefore we prefer the value 1.51 as the best compromise for all the data and for the relatively large and homogeneous HIFLUGCS sample as our prime value.

For the work in this paper we calculate the predicted luminosity function for the median redshift of the REFLEX II cluster sample of  $z = 0.102$  and quote the corresponding cosmological parameters for  $z = 0$ . For the modeling of these two different epochs we use the standard formulae for the linear growth of the density fluctuation field, since it is the linear fluctuation evolution that is accounted for in the applied statistical theory.

With these ingredients we can predict the X-ray luminosity function analytically for different cosmological models. Note that for any variation of the cosmological model away from our

**Table 2.** Default cosmological model parameters.

parameter	explanation	value
$h_{100}$	Hubble parameter	0.7
$\Omega_b$	baryon density	0.045
$n_s$	Primordial P(k) slope	0.96
$\alpha_{sl}$	$L_X - M$ relation slope	1.51
$n_0$	$L_X - M$ relation norm.	0.1175
mass bias	X - ray mass underestimation	0.1

**Notes:** In addition to the parameters we assume the model to describe a flat  $\Lambda$ CDM Universe.

reference model, we have to convert the input X-ray luminosities, and the values of  $V_{max}$  with the corresponding survey selection function, and the scaling relations to the new cosmology.

## 5. Cosmological parameters from the REFLEX X-ray luminosity function

To determine the cosmological model parameters which best fit our observations we use a Likelihood function method in an analogous way to that used for the fitting of the Schechter function in section 3.1. We are comparing again the predicted and observed distribution function of X-ray luminosities, since this is very close to an observable, as the spectral model assumptions used for their derivation introduce only negligible new uncertainties except for changes in the assumed geometry of the universe which are taken into account. Thus we derive the following predicted distribution function which now also accounts for the scatter in the  $L_X - M$  scaling relation

$$\lambda(L_X) = \int n(L'_X) V_{surv}(L'_X) \Phi(L''_X, L'_X) \Psi(L'_X, L_X) dL''_X dL'_X \quad (11)$$

where  $n(L_X) = \frac{dn(L_X)}{dL_X}$  is the differential X-ray luminosity function and  $V_{surv}$  is the volume in which clusters with luminosity  $L_X$  can be found. In case of no redshift constraints the latter is equal to  $V_{max}$ , while  $\Phi(L''_X, L'_X)$  is the scatter in the  $L_X - M$  relation and  $\Psi(L'_X, L_X)$  is the uncertainty of the flux or luminosity measurement.

Fig. 7 shows the observed X-ray luminosity function compared to the best fitting model prediction, where only clusters with  $L_X \geq 0.25 \times 10^{44} h_{70}^{-2} \text{ erg s}^{-1}$  and  $z \leq 0.4$  have been used in the fit. This involves in total 698 clusters including the lower total count limit of 20 source photons. Over the fitted range the two functions show a very good agreement. The reason for using a restricted luminosity range for this fit is the fact, that for lower values of  $L_X$ , which corresponds to the regime of galaxy groups, we have no reliable constraints on the  $L_X - M$  relation. It is too dangerous to rely on the assumption that the relation is a straight power law over the full range of observed X-ray luminosities.

In this section we are primarily interested in studying the constraints on those cosmological parameters, for which we can get the most interesting information, that is  $\Omega_m$  and  $\sigma_8$ . We therefore keep other parameters fixed, but we use a Hubble constant of  $h = 0.7$ , a flat universe, a baryon fraction compared to the critical density of 0.045, and a spectral index of the primordial matter density fluctuation power spectrum of 0.96. In addition we assume the Universe to be flat, described by a  $\Lambda$ CDM model, that is a Dark Energy universe with an equation of state parameter  $w = -1$ . These values are chosen to be consistent with the

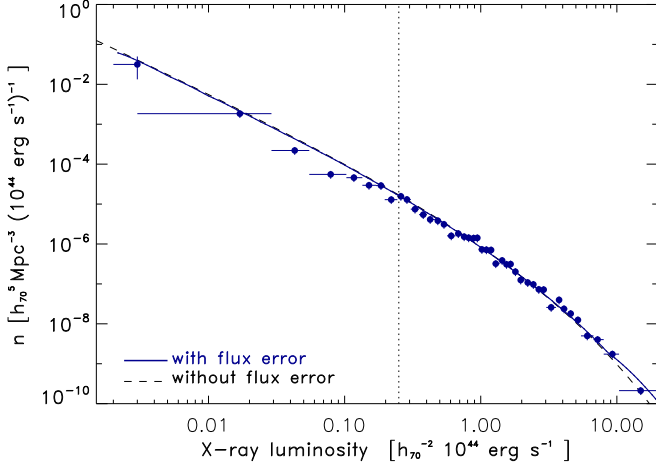


**Fig. 7.** X-ray luminosity function of REFLEX II (data points) and the predicted X-ray luminosity function for the best fitting cosmological model.

9-year WMAP results and with the PLANCK results (Hinshaw et al. 2012, Planck Collaboration 2013b), except for the Hubble constant which is reported to be determined as  $67.8 \pm 0.77$  for the combined results in the PLANCK publication. We also use a mass bias factor of 0.9 which accounts for the effect that the X-ray determined mass, which is the base of the  $L_X - M$  relation in Eq. 10, may be biased low compared to the true mass by about 10%. This has been found in simulations (Nagai et al. 2007, Valdarnini & Piffaretti 2010, Meneghetti et al. 2010) and in comparison to weak lensing results (Mahdavi et al. 2013, Zhang et al. 2010, Okabe et al. 2010). The assumed parameters are summarized in Table 2. We explore the effect of some of these assumptions in a subsequent section.

With these model assumptions the best constraints for the parameters  $\Omega_m$  and  $\sigma_8$  are shown in Fig. 8. We show two results for the significance limits, one for the preferred slope of the  $L_X - M$  scaling relation of 1.51 and a second set of contours for a slope value of 1.61. Table 3 summarizes the fitting results. The uncertainties quoted here are only the statistical uncertainties for the constraints on these two parameters alone. There is some degeneracy of the two parameters indicated by the elongated error ellipses, but due to the well described shape of the X-ray luminosity functions both parameters can be well constrained. Fig. B.1 in the Appendix provides an explanation for the behaviour of the constraints of  $\Omega_m$  and  $\sigma_8$ . An increase of  $\Omega_m$  increases the amplitude of the X-ray luminosity function over the entire luminosity range, this can be partly compensated by lowering  $\sigma_8$ , but this affects mostly the high luminosity part. This partial compensation leads to the elongated error ellipses, but also allows the degeneracy to be broken.

The lower panel of Fig. B.1 in the Appendix shows the changes of the predicted XLF with the change of the slope of the  $L_X - M$  relation. A steeper slope of the relation results in a shallower slope of the X-ray luminosity function. From this behaviour we can predict the change in the best fitting cosmological parameters. A steeper slope of the  $L_X - M$  relation can be counteracted by lowering  $\sigma_8$  with an additional higher value of  $\Omega_m$  to adjust the normalization. This is what we observe in Fig. 8.

**Table 3.** Fit parameters of the best fitting cosmological model prediction to the REFLEX II X-ray luminosity function.

fit	$L_X - M$ slope	$\Omega_m$	$\sigma_8$
$L_X \geq 0.25$	1.51	$0.27 \pm 10\%$	$0.80 \pm 3.5\%$
$L_X \geq 0.25$	1.61	$0.31 \pm 10\%$	$0.73 \pm 3.5\%$
$L_X \geq 0.25$	marginalized	$0.29 \pm 14\%$	$0.77 \pm 9\%$

**Notes:** The first column shows the luminosity range used in the fit, while the redshift range is  $z \leq 0.4$ . The second column gives the slope of the  $L_X - M$  relation used in the fit for the model prediction of the XLF. For the results in the third line we have marginalized over the slope and normalisation of the scaling relation.

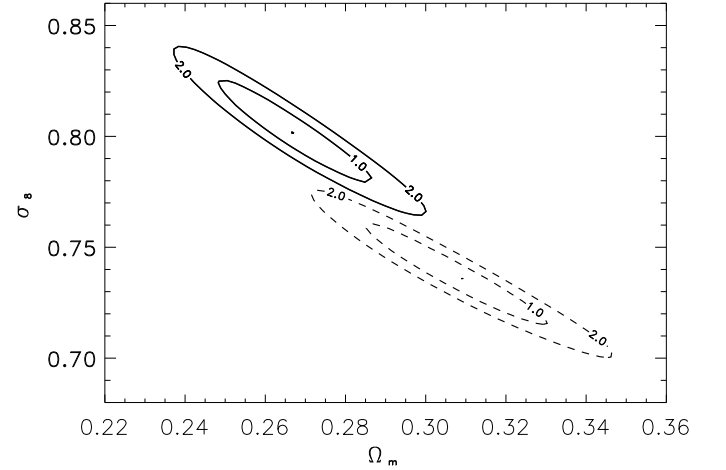


**Fig. 8.** Constraints of the cosmological model parameters  $\Omega_m$  and  $\sigma_8$  from the comparison of the observed REFLEX II X-ray luminosity distribution and the cosmological model predictions. Two results are shown for an  $L_X - M$  relation slope of 1.51 (upper ellipses) and 1.61 (lower dashed ellipses). The contour lines show 1 and  $2\sigma$  confidence limits.

## 6. The role of scaling relations

In the last section we already discussed the influence of the slope of the scaling relation on the cosmological fitting results. A closer inspection of the effect of varying the different model parameters for the fits to the observational data clearly shows that the uncertainties in the observable - mass scaling relation is the most severe bottle-neck in deriving cosmological constraints from our cluster survey. In Fig. 9 and Table 4 we show the effect of the different parameters characterizing the  $L_X - M$  scaling relation used in our modelling. The parameters are the normalization, the slope, and the scatter in the relation. A change in the slope has clearly the largest effect. It moves the result in a direction very close to the major axis of the error ellipse. A change in the normalization has a less dramatic consequence, but it moves the result in an almost perpendicular direction, more along the minor axis of the error ellipse. Also the scatter has a non-negligible effect on the results. We list the changes in the best fitting model parameters as an effect of changes of the scaling relations in Table 4 in terms of fractional changes and logarithmic derivatives. Since the effect of the uncertainty in the measured flux is the same as that of the scatter of the scaling relations (see Eq. 11), we also give the result for the fractional



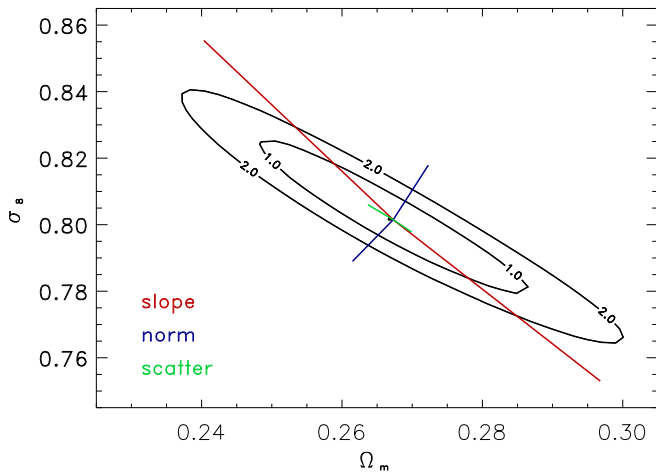


**Fig. 9.** Variation of the best fitting parameters for  $\Omega_m$  and  $\sigma_8$  with a change in slope, scatter and normalization of the  $L_X - M$  scaling relation. The end and mid points of the bars give the results for the following values, respectively: slope = 1.435, 1.51, 1.586 ( $\pm 5\%$ , largest bars), normalization = 0.1292, 0.1175, 0.1058 ( $\pm 10\%$ , bars in direction of minor axis), scatter = 27%, 30%, 33% ( $\pm 10\%$ , smallest bars).

change of the combination of the two parameters (assuming that Gaussian error addition applies).

To include these uncertainties for the slope and amplitude of the scaling relation as the most critical parameters into our cosmological constraints, we perform a fit marginalizing over both parameters. We allow approximate  $1\sigma$  uncertainties of 7% for the slope and 14% for the normalization. The uncertainty in the mass bias is equivalent to a corresponding uncertainty in the normalization. Thus this error includes both, the amplitude error of the relation of  $\sim 10\%$  and a 10% mass bias uncertainty. The uncertainty of  $\pm 7\%$  for the slope of the scaling relation is motivated by the difference of the most reliable results in the literature: the statistically complete HIFLUGCS sample with  $\alpha_{sl} = 1.46$ , Pratt et al. (2009) BCES (Y|X) fit with  $\alpha_{sl} = 1.53$ , and Vikhlinin et al. (2009) with  $\alpha_{sl} = 1.61$ . These studies use galaxy cluster samples constructed to be representative of the relevant survey population. We thus take the mean difference of these results as the sigma for the slope variation. We also note that the statistical uncertainties of the slopes quoted in these works is of similar magnitude as this difference.

Fig. 10 shows the new constraints with relaxed assumptions for the two most critical parameters. The contours enclose a larger area than those of Fig. 8. The  $2\sigma$  contour is now embedding both error ellipses shown in Fig. 8. One behaviour is noteworthy. The fit of the X-ray luminosity distribution favours a slightly higher value for the slope than 1.51 for the best match of the observed and predicted X-ray luminosity distribution. This shifts the center of the uncertainty ellipses slightly towards the lower right corner of the plot, the direction of the result for a larger slope. The numerical values of the results are given in Table 3.

## 7. Other systematic uncertainties

As already mentioned it is not the aim of this paper to provide a comprehensive marginalization over all uncertainties involved in our analysis since we like to defer this task to a following publication which uses a more appropriate approach. We rather

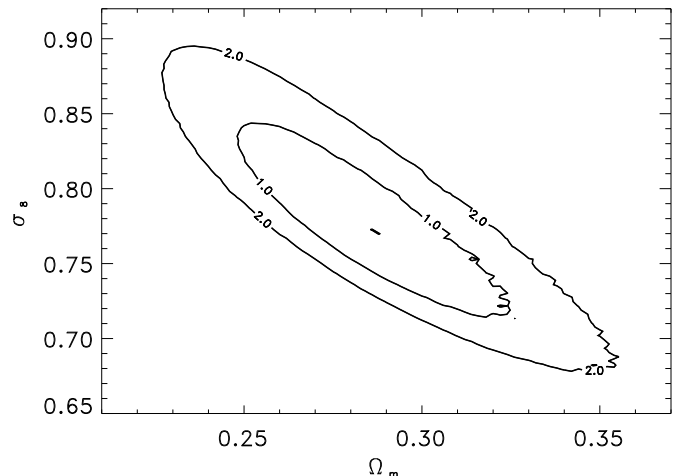


**Fig. 10.** Constraints of the cosmological model parameters  $\Omega_m$  and  $\sigma_8$  for the REFLEX II cluster sample with a marginalization over the most influential model parameters involving the slope,  $\alpha_{sl}$ , and the normalization,  $n_0$ , of the  $L_X - M$  relation. Shown are the 1 and  $2\sigma$  confidence limits.

like to make the effect of the isolated variation of the important parameters transparent. Therefore we studied the dependence of the results for  $\Omega_m$  and  $\sigma_8$  on the variation of other cosmological parameters. The results are summarized in Table 4. A parameter with a large effect is the Hubble constant,  $H_0$ . For constant  $\Omega_m$  a change in the Hubble constant changes the mean density of the Universe and thus it also changes the filter scale (in Eq. 7) for a cluster of given mass. This explains only part of the effect of  $H_0$ , as we found that a change in  $H_0$  cannot be compensated by a corresponding change in  $\Omega_m$ . The effect of  $H_0$  is more complex. While the baryon density in the Universe, a possible curvature, and the equation of state parameter  $w$  have a very minor influence, the slope of the primordial power spectrum,  $n_s$ , is also an important parameter to take into account. Finally, the role of  $f_{mass}$  was already discussed, since its effect is the same as that of changing the  $L_X - M$  normalisation, as can be seen from Eq. 10.

We have also checked the effect of sample incompleteness on the results of the cosmological constraints by arbitrarily excluding a fraction of the observed clusters from the sample analysed. The effect of a reduction of the sample by 10% for example decreases  $\Omega_m$  by 3.5% and  $\sigma_8$  by increases by less than 0.2%. Thus it is clear that at this stage the sample completeness, which is very high for REFLEX II, is of no concern for the results discussed here.

An inspection of Table 4 shows again that the most dramatic effect on the results comes from the uncertainty of the slope of the  $L_X - M$  scaling relation, while the effect of the normalisation is among the next most important parameters together with  $H_0$  and  $n_s$ . Therefore we are confident that the marginalization over these two most important parameters gives a fair and conservative account of the overall uncertainty of our cosmological constraints.

The relatively smaller effect of these other cosmological parameters on the  $\Omega_m$  and  $\sigma_8$  parameters compared to the uncertainties of the scaling relation was e.g. also discussed in Voevodkin & Vikhlinin (2004), Vikhlinin et al. (2009), Henry et al. (2009) and Rozo et al. (2010) with the same conclusion.

**Table 4.** Dependence of the best fitting values for the cosmological parameters  $\Omega_m$  and  $\sigma_8$  on the choice of other model parameters.

parameter	$\frac{d\ln\Omega_m}{d\ln P}$	$\frac{d\ln\sigma_8}{d\ln P}$	$\Delta P$	$\Delta\Omega_m$	$\Delta\sigma_8$
$\alpha_{sl}$	2.2	-1.3	10%	22%	13%
$n_0$	-0.22	-0.18	10%	-2.2%	-1.8%
scatter	0.12	-0.05	10%	1.2%	-0.5%
scatter + ferr.	0.16	-0.07	10%	1.6%	-0.7%
$H_0$	-0.7	0.4	5%	-3.5%	2%
$\Omega_b$	0.15	-0.07	10%	1.5%	-0.7%
$n_s$	-0.9	0.5	5%	-4.5%	2.5%
$\Omega_m + \Omega_\Lambda$	$\leq \pm 0.11^a$	$\leq 0.07$	5%	$\leq \pm 0.5\%$	$\leq 0.35\%$
$f_{mass}$	-0.3	-0.28	10%	-3%	-3%
$w$	$\leq 0.02$	$\geq -0.02$	10%	0.15%	-0.19%

<sup>a)</sup>  $\Omega_m$  decreases with a change of curvature in both directions.

**Notes:** The parameters for the  $L_X - M$  scaling relation are the slope  $\alpha_{sl}$ , the normalization,  $n_0$ , and the scatter. We also show the effect of the variation of the combined scatter and flux error. The cosmological parameters in the second part of the Table are  $H_0$ , the Hubble constant,  $\Omega_b$  the baryon density, and  $n_s$  the slope of the primordial power spectrum.  $\Omega_m + \Omega_\Lambda$  gives with the degree of the deviation from one the deviation from a flat universe,  $f_{mass}$  provides the mass bias, the correction from the X-ray determined hydrostatic mass to the true mass of the clusters, and  $w$  shows the effect of a constant equation of state parameter for Dark Energy.  $P$  in the formulas for the columns indicates the parameter of the row.  $\Delta\Omega_m$  and  $\Delta\sigma_8$  give the change of the resulting values for these two cosmological parameters upon a parameter variation of  $\Delta P$ .

## 8. Discussion and comparison to previous results.

A comparison of the results on the cosmological parameter constraints shown in Fig. 8 and Fig. 10 clearly shows how much information is lost due to our imprecise knowledge of the observable - mass scaling relations. Therefore one of our major efforts in the future will be invested to improve this situation.

One effect not included in the error bars of the XLF given here is the sample variance. This effect is caused by structure on very large scales such that our survey results would be slightly different would the data have been sampled in exactly the same way in a different region of our Universe. We estimated the cosmic variance in the same way as done in our previous paper of the XLF of REFLEX I (Böhringer et al. 2002) by approximating the survey volume by a sphere. We then calculate the variance of the dark matter density from the power spectrum filtered by a top hat filter with the size of this sphere. This approach and its effects are also described by Hu & Kravtsov (2003). To further estimate the variance effect on the cluster density we also have to account for the fact that the cluster density is biased with respect to the dark matter. The bias factor depends on the X-ray luminosity or the mass of the clusters. The calculations of the bias are based in the formulas by Tinker et al. (2010) and have been described in Balaguera-Antolinez et al. (2011). We find that the sample variance dominates the uncertainties in the cluster density in the XLF at  $L_X < 8 \times 10^{42} h_{70}^{-2} \text{ erg s}^{-1}$ . It is less than half at  $L_X \sim 2.5 \times 10^{43} h_{70}^{-2} \text{ erg s}^{-1}$ , the lowest luminosity included in our fits, and it decreases rapidly thereafter. Thus we have not corrected for this effect in the present work.

With our conservative approach of marginalization over the most important systematic uncertainties, we can now compare our results to other cosmological studies using galaxy clusters.

The result most similar in the nature of the constraints is the recently published result obtained with galaxy clusters detected in the PLANCK microwave background survey through the Sunyaev-Zel'dovich effect (SZE, Planck Collaboration 2013a). This survey is also an all-sky survey. There are 189 galaxy clusters detected at high signal/noise used for the cosmological analysis. 92% of the clusters have redshifts  $z \leq 0.4$  and 81% have  $z \leq 0.3$  compared to our REFLEX II sample where 99% have  $z \leq 0.4$  and 92%  $z \leq 0.3$ . Thus even though the REFLEX II sample has on average lower redshifts, the redshift range is still quite similar. The cosmological analysis for the PLANCK clusters uses a different approach than the one used here. While we have reproduced the luminosity distribution, in the PLANCK analysis the redshift distribution is used to determine the best fit. In the absence of strong evolutionary effects in the galaxy cluster population for the small redshift range, the approaches have in effect some similarity. In the probed redshift range in the nearby Universe, the PLANCK cluster sample is approximately flux limited, as the measured integrated SZE is proportional to the apparent surface area of the objects which is decreasing with the inverse square of the distance for low redshifts. A redshift histogram at low redshift thus reflects the cumulative luminosity function probed at different luminosity cuts. In this sense the two approaches are quite comparable.

There is another similarity between the two surveys. The mass-observable relation for the SZE detected PLANCK clusters relies heavily on the calibration of the X-ray properties of the clusters (see Arnaud et al. 2010, Melin et al. 2011, and Planck Collaboration 2013a). Therefore we actually expect to see constraint results which give a very similar parameter range. Since systematic effects are more important at this current state, the larger size of the REFLEX II sample does not play a major role. Therefore it is on one hand not very surprising to see such a good agreement between the cosmological constraints from the two surveys as shown in Fig. 11. On the other hand the cluster detection and selection is very different and the agreement gives much support to the different survey methods.

In Fig. 11 we also compare the cluster results for the constraints on  $\Omega_m$  and  $\sigma_8$  to those derived from the analysis of the microwave background anisotropies as measured with WMAP 9yr data (Hinshaw et al. 2013) and by the PLANCK mission (Planck Collaboration 2013b). As discussed in detail in the PLANCK result paper on cosmological constraints from galaxy clusters (Planck Collaboration 2013a), the two results from PLANCK show some discrepancy. Here we confirm the PLANCK cluster results from X-ray observations very well, using a somewhat different approach based on the luminosity distribution instead of the redshift distribution of the clusters. In Fig. 11 we show the best cosmological fit for PLANCK CMB data with WMAP polarization data quoted in the PLANCK cosmology paper (Planck Collaboration 2013b) with  $1\sigma$  error bars. Note that this result is closer to the cluster constraints than the error ellipses shown in Planck Collaboration (2013a).

How difficult it is to make our results compatible with the PLANCK CMB constraints is illustrated in Fig. 12. There we show the predicted X-ray luminosity function for the PLANCK CMB cosmology compared to the one observed in the REFLEX II survey. The dramatic difference in cluster number counts is apparent. It was already discussed in the PLANCK paper on cosmological results from clusters (Planck Collaboration 2013a) that the results could very roughly be reconciled by allowing a mass bias of 45% (that is assuming that the X-ray mass determination covers on average only 55% of the true mass of a cluster). This assumption is included in the result shown in Fig. 12. It gives a

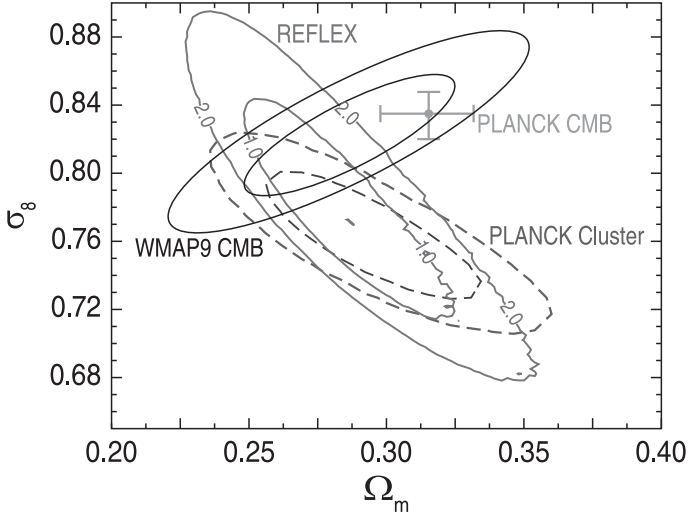


**Fig. 11.** Comparison of the marginalized cosmological model constraints for the REFLEX II survey with the results from the PLANCK Mission for galaxy clusters (Planck Collaboration 2013a) as well as with the cosmic microwave background (CMB) power spectrum (Planck Collaboration 2013b) and with the CMB results from the 9-year WMAP data (Hinshaw et al. 2013). The contour lines give the 1 and  $2\sigma$  results for the cluster surveys and WMAP mission and the cross gives the  $1\sigma$  result from PLANCK CMB (Planck Collaboration 2013b).

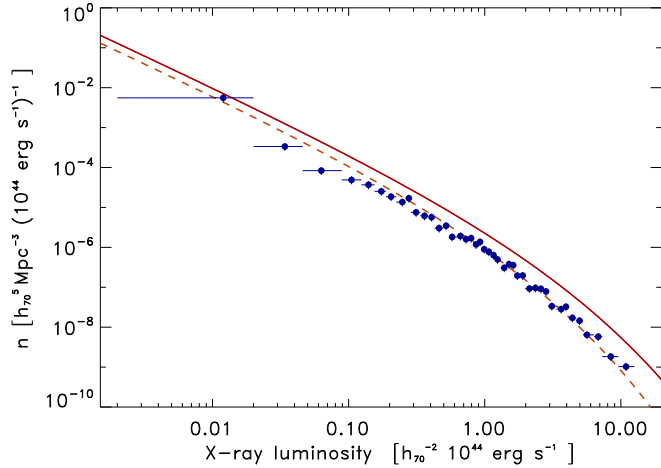


**Fig. 12.** Comparison of the observed REFLEX II luminosity function (data points) with the theoretical prediction for the best fitting model to the PLANCK CMB data (Planck Collaboration XVI 2013b) with  $\Omega_m = 0.315$  and  $\sigma_8 = 0.834$  with a mass bias of 10% (upper solid line). Same calculation but assuming a mass bias of 45% is shown by the lower dashed line.

rough agreement, but the value for the mass bias is far outside the range of acceptable values. In the comparison of X-ray determined masses with mass measurements from gravitational lensing (Mahdavi et al. 2013, Zhang et al. 2010, Okabe et al. 2010), one finds small biases with X-ray masses lower by few percent to about 20%. The large mass bias needed above is not compatible with these observational results. We also note in Fig. 11 that the cluster result has an overlap with the WMAP CMB data.

We can also compare our results with previous X-ray cluster studies by Vikhlinin et al. (2009), Henry et al. (2009), and

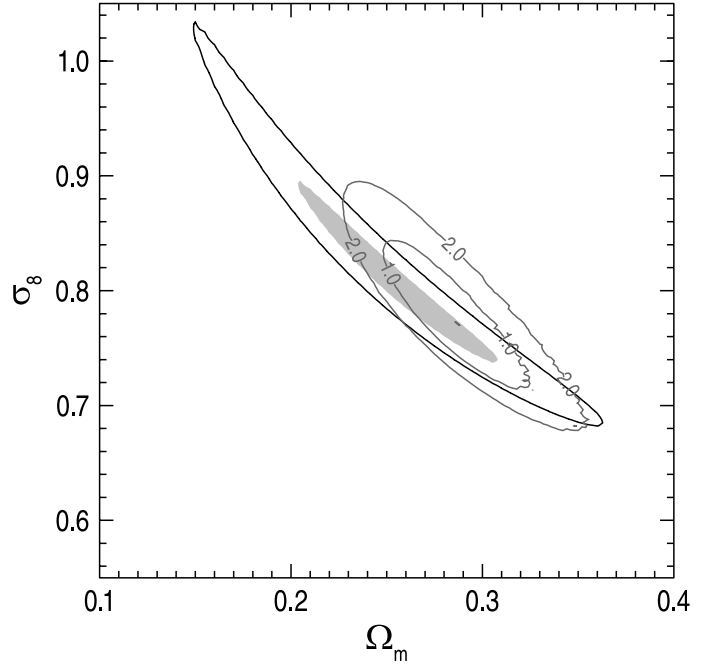


**Fig. 13.** Comparison to the results from the X-ray cluster survey by Vikhlinin et al. (2009). The constraints on  $\Omega_m$  and  $\sigma_8$  shown here have been derived from the low redshift sample of 49 clusters at  $\langle z \rangle \sim 0.05$  of their survey. 1 and  $2\sigma$  contours are shown for both surveys.

Mantz et al. (2008). The cosmological analysis of Vikhlinin et al. (2009) is based on a nearby sample of 49 clusters selected from the brightest clusters in the sky with  $\langle z \rangle \sim 0.05$  and a more distant cluster sample of 37 clusters from the 400 deg<sup>2</sup> survey (Burenin et al. 2007) with  $\langle z \rangle \sim 0.55$ . All clusters are well observed with Chandra so that masses can be estimated from low scatter mass proxies like gas mass,  $M_{gas}$ , and the product of gas mass and bulk temperature,  $Y_X$ . While the full set of data is used to obtain information on the equation of state parameter of Dark Energy,  $w$ , the parameters  $\Omega_m$  and  $\sigma_8$  are best constrained by the low redshift sample only, as discussed in their paper. In Fig. 13 we compare their results to ours and find very good agreement. Our results are better constrained along the degeneracy direction, due to the better information we have on the shape of the XLF.

Also the work by Henry et al. (2009) uses a small sample of local clusters with a better mass proxy than X-ray luminosity, which is the spectroscopically measured intracluster medium temperature from X-ray observations. Their sample comprises 48 of the brightest clusters in the sky (from HIFLUGCS, Reiprich & Böhringer 2002) with temperatures measured with the ASCA Satellite taken from Horner et al. (2001) and Ikebe et al. (2002) with  $z \leq 0.2$  and  $k_B T \geq 3$  keV. The results obtained by marginalizing over 12 uninteresting parameters are characterized by very elongated error ellipses (see their Fig. 10) for which the authors provide the parameterization,  $\sigma_8 \left(\frac{\Omega_m}{0.32}\right)^{0.3} = 0.86(\pm 0.04)$ . Our results shown in Fig. 10 are best characterized by  $\sigma_8 \left(\frac{\Omega_m}{0.27}\right)^{0.57} = 0.80(\pm 0.03)$ . Transforming both relations to the same pivot point in the middle, we find:  $\sigma_8 \left(\frac{\Omega_m}{0.30}\right)^{0.3} = 0.877(\pm 0.04)$  for the results of Henry et al. (2009) and  $\sigma_8 \left(\frac{\Omega_m}{0.30}\right)^{0.57} = 0.753(\pm 0.03)$  for our work. It displays an offset between the two results of almost  $2\sigma$ . The data used by

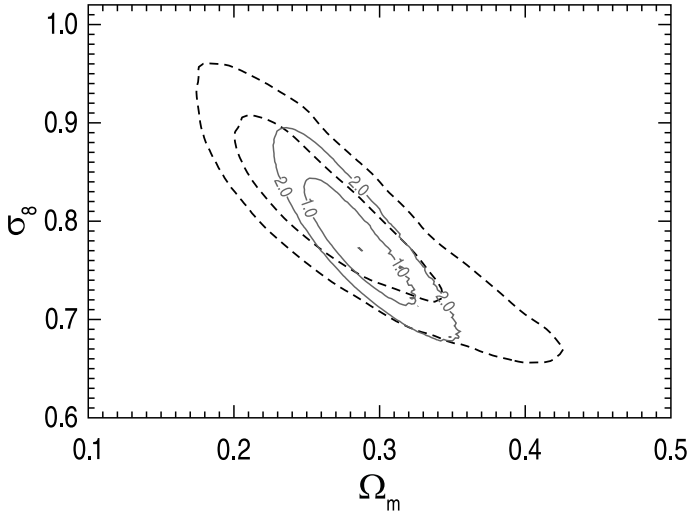


**Fig. 14.** Comparison to constraints from SDSS MaxBCG clusters (Roza et al. 2010). The more than 10 000 clusters cover a redshift range of  $z = 0.1 - 0.3$  and an approximate mass range of  $M = 7 \times 10^{13} - 2 \times 10^{15} M_{\odot}$ .

Herny et al. (2009) stem from the pre-Chandra/XMM-Newton era without good spatially resolved spectroscopy. Thus the small difference between these results and ours is not a reason for concern.

Mantz et al. (2008) use for their analysis 130 clusters from REFLEX I with a lower luminosity cut of  $L_X = 2.55 \times 10^{44} h_{70}^{-2} \text{ erg s}^{-1}$  in the 0.1 - 2.4 keV band, 78 clusters from the northern BCS sample, and 34 clusters from MACS with a flux limit of  $F_X = 2 \times 10^{-12} \text{ erg cm}^{-2} \text{ s}^{-1}$ . The cosmological constraints on the two parameters  $\Omega_m$  and  $\sigma_8$  from an analysis of the cluster data alone marginalizing over a comprehensive set of other parameters is shown in their Fig. 7. Our error ellipse from Fig. 10 falls nicely in the middle of their constraints region. At  $\Omega_m = 0.27$  their constraints are  $\sigma_8 = 0.805 \pm 0.1$  for example in very close agreement to our results.

Roza et al. (2010) derived constraints for cosmological parameters from an analysis of the galaxy cluster population in the Sloan Digital Sky Survey (SDSS) obtained by means of the MaxBCG cluster detection method (Koester et al. 2007). 10810 galaxy cluster are used in the redshift range  $z = 0.1 - 0.3$  from a survey area of  $7398 \text{ deg}^2$  of SDSS-DR4+. While the number of clusters of the sample is much larger than that from any other survey discussed here, the scatter in the richness - mass relation is much larger than for the X-ray related mass proxies. The richness mass relation is calibrated by an analysis of gravitational lensing data of stacked cluster shear profiles from SDSS. In Fig. 14 we compare our results to their constraints noting a very good overlap.

In Fig. 15 we then compare our results to a set of the X-ray and optical results discussed above, where the constraints from the literature have further been tightened by combining the cluster constraints with those of WMAP 5yr data (Dunkley et al. 2007). For the display of our results we use our preferred  $L_X - M$  scaling relation from Fig. 8 neglecting the uncertainties of this relation. We note that this relation shows perfect consistency with the other cosmological data. Thus using the further constraints from the cosmic microwave background anisotropies we are pointed towards an observable - mass relation for our clusters which agrees very well with the default relation used in this paper.

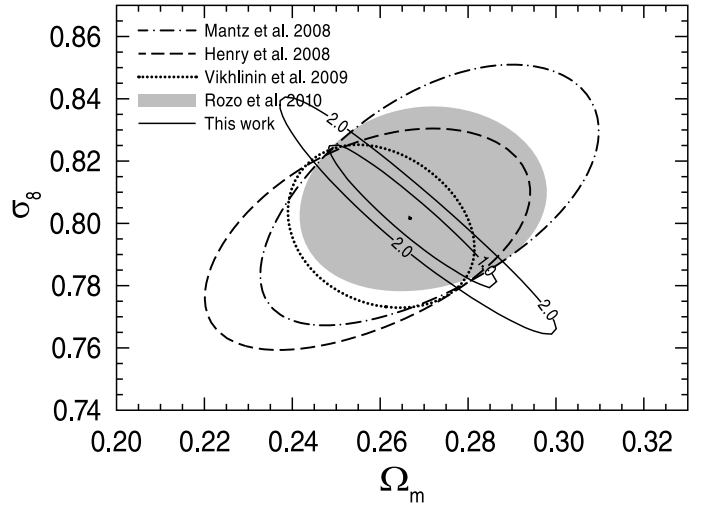


**Fig. 15.** Comparison to optical and X-ray surveys, where the data have been combined with WMAP 5yr data (Roza et al. 2010, Mantz et al. 2008, Vikhlinin et al. 2009, Henry et al. 2009). Our data are the REFLEX constraints with no marginalization over scaling relation systematics. The contours for the literature data give 68% confidence limits and for the REFLEX II data 1 and  $2\sigma$  contours are shown.

In our work, the good characterization of the shape of the XLF is the means to break the degeneracy between the  $\sigma_8$  and  $\Omega_m$  parameter. Another way to get a better separation between the two parameters is to extend the cluster study to higher redshifts. This has been recently achieved in ground based microwave surveys, detecting clusters in the SZE. Thus to compare our findings to their results provides another independent consistency check for our approach. From the cluster sample detected with the South Pole Telescope (SPT) Benson et al. (2013) obtained cosmological parameter constraints from 18 massive clusters in the redshift range  $z = 0.3$  to 1.1. Our constraints fall very nicely into the middle of their constraints using an  $H_0$  prior and Big Bang Nucleosynthesis results. Our results also overlap well with the combined constraints of SPT cluster and WMAP CMB data. The other distant SZE cluster sample comes from the microwave background survey with the Atacama Cosmology Telescope (ACT). Cosmological constraints have recently been derived by Hasselfeld et al. (2013) from 15 massive clusters in the redshift range  $z = 0.2 - 1.4$ . Our results overlap well with their constraints in the lower half of their contours at lower  $\sigma_8$ .

## 9. Summary and conclusions

We used the REFLEX II catalog and the well defined selection function to construct the X-ray luminosity function for the sample at a median redshift of  $z = 0.102$ . For the flux limit of  $F_X = 1.8 \times 10^{-12} \text{ erg s}^{-1} \text{ cm}^{-2}$ , a luminosity limit of  $L_X = 0.03 \times 10^{44} \text{ erg s}^{-1}$  (for 0.1 - 2.5 keV), a lower photon count limit of 20 source photons, and a redshift range of  $z = 0 - 0.4$ , some 819 clusters are included in the luminosity function determination. The cluster catalog is better than 90% complete, with a best estimate of about 95% as detailed in Böhlinger et al. (2013) and we also expect a few percent contamination by clusters whose X-ray luminosity may be boosted by an AGN. Since this fraction is small and as an incompleteness even of the order of 10% causes only little change in the derived cosmological parameters

as detailed in section 7, we have not included any correction for incompleteness in the presented results.

Inspecting the XLF in different redshift shells reveals no significant evolution of the XLF. We showed for our best fitting cosmological model that this undetectable change is consistent with the theoretical expectation. This does not imply that there is no evolution in the cluster mass function. There are two competing effects, the evolution of the mass function and the evolution of the  $L_X - M$  relation. The relation of X-ray luminosity to mass evolves as clusters have been more compact on average in the past which increases the X-ray luminosity (through the square-law dependence on the density) and clusters of the same mass become brighter. This compensates for the loss of massive clusters at higher redshifts and suppresses the evolution in X-ray luminosity.

In search of a good analytical description of the XLF, we found that the Schechter function does not capture our knowledge with sufficient precision. We therefore propose a modified Schechter function for a good description of the data.

The most interesting application of the XLF is to test theoretical predictions of this function within the frame of different cosmological models. These tests are based on the theory of cosmic evolution and structure formation and rely among other things on the description of the transfer function of the power spectrum by Eisenstein & Hu (1998), on the numerical simulation calibrated recipe for the cluster mass function by Tinker et al. (2008), and on scaling relations that enable the connection of cluster mass and X-ray luminosity. Apart from the scaling relations, the other theoretical framework has been intensively tested and is believed to be accurate at about the 5% level.

We find that we can get a very good match of the observed XLF with the theoretical predictions for a very reasonable cosmological model; in particular if we restrict the fitting to the luminosity range  $L_X \geq 0.25 \times 10^{44} \text{ erg s}^{-1}$  (0.1 - 2.4 keV) where we have an observationally calibrated  $L_X - M$  relation (note the good match of the predicted and observed XLF in Fig. 7). In using the observational data to constrain cosmological parameters we have in this paper not pursued a comprehensive marginalization over all relevant parameters. We postpone this to later work. We rather wanted to gain an overview and an understanding of the effect of the different parameters by studying them individually. From this investigation it becomes clear that by far the largest uncertainty in the constraints of cosmological parameters is introduced by the  $L_X - M$  scaling relation and specifically its slope and normalization. We give a detailed account on the influence of the other parameters and then concentrate on a marginalization study including these two most important input parameters, which provides a good account of the overall uncertainties. The important constraints that we derive from the REFLEX II data are in the matter density parameter  $\Omega_m = 0.29 \pm 0.04$  and the amplitude parameter of the matter density fluctuations  $\sigma_8 = 0.77 \pm 0.07$ .

The currently most interesting comparison of our findings with other results is that with the recently published cosmological constraints from clusters detected with PLANCK (Planck Collaboration 2013b). The PLANCK results show a tension between the cosmological constraints on  $\Omega_m$  and  $\sigma_8$  from clusters and from the cosmic microwave background (CMB) anisotropies, which has caused a lively debate. We find that our results agree perfectly with the PLANCK cluster data and it would be very hard to reconcile them with the CMB derived results. However, we find that our results are consistent with the constraints from the CMB study with WMAP (Hinshaw et al. 2013). Since there is also some tension between the implications from the CMB data of WMAP and PLANCK, the source

of which is currently under investigation, we are confident, that the solution of these problems will bring a closer agreement of all the data in the future without a significant change of our results.

The good agreement of our results with the recent work on cluster cosmology in the literature is encouraging. But we should point out here that our new results provide tighter constraints on the two tested parameters than the previous studies and constitute a significant improvement. We have, however, reached a limit where a further increase of the clusters sample and of the overall statistics will not lead to much further improvements, if we cannot better calibrate the scaling relations. A major reason for our poor knowledge on the scaling relations originates in several facts. On one hand the cluster samples with very well defined selection criteria used in the scaling relation studies are still very small with typically 30 - 50 objects. Another source of uncertainty is revealed by the difference in results for mass, temperature, or X-ray luminosity determined for the same set of clusters by different authors (e.g. Reichert et al. 2011). And there are still some calibration uncertainties for the XMM-Newton and Chandra instruments for which there is an ongoing effort of their resolution (e.g. Kettula et al. 2013). Therefore one of the next major efforts of the authors will be to increase the sample size and the data reduction quality of the cluster samples to obtain better constraints on the important scaling relations.

*Acknowledgements.* We like to thank the ROSAT team at MPE for the support with the data and advice in the reduction of the RASS and the staff at ESO La Silla for the technical support during the numerous observing runs conducted for the REFLEX project since 1992. Special thanks goes to Peter Schuecker, who was a very essential part of our team and who died unexpectedly in 2006. H.B. and G.C. acknowledge support from the DFG Transregio Program TR33 and the Munich Excellence Cluster "Structure and Evolution of the Universe". C.A.C. acknowledges STFC for financial support.

## References

- Allen, S.W., Schmidt, R.W., Fabian, A.C., et al., 2003, MNRAS, 342, 287  
 Allen, S.W., Evrard, A.E. & Mantz, A.B., 2011, ARA&A, 49, 409  
 Arnaud, M., Pratt, G.W., Piffaretti, R., et al., 2010, A&A, 517, 92  
 Balaguera-Antolínez, A., Sanchez, A., Böhringer, H., et al., 2011, MNRAS, 413, 386  
 Balaguera-Antolínez, A., Sanchez, A., Böhringer, H., et al., 2012, MNRAS, 425, 2244  
 Benson, B.A., de Haan, T., Dudley, J.P., et al., 2013, ApJ, 763, 147  
 Böhringer, H., Voges, W., Huchra, J.P., et al., 2000, ApJS, 129, 435  
 Böhringer, H., Schuecker, P., Guzzo, L., et al., 2001, A&A, 369, 826  
 Böhringer, H., Collins, C.A., Guzzo, L., et al., 2002, ApJ, 566, 93  
 Böhringer, H., Schuecker, P., Guzzo, L., et al., 2004, A&A, 425, 367  
 Böhringer, H., Schuecker, P., Pratt, G.W., et al., 2007, A&A, 469, 363  
 Böhringer, H., Pratt, G.W., Arnaud, M., et al., 2010, A&A, 514, 32  
 Böhringer, H., 2011, AIP Conf. Proceedings, 1381, 137  
 Böhringer, H., Dolag, K., Chon, G., 2012, A&A, 539, 120  
 Böhringer, H., Chon, G., Collins, C.A., et al., 2013, A&A, 555, A30  
 Borgani, S., Rosati, P., Tozzi, P., et al., 2001, ApJ, 561, 13  
 Burenin, R.A., Vikhlinin, A., Hornstrup, A., et al., 2007, ApJS, 172, 561  
 Burke, D.J., Collins, C.A., Sharples, R.M., et al., 1997, ApJ, 488, L83  
 Burns, J.O., Ledlow, M.J., Loken, C., et al., 1996, ApJ, 467, L49  
 Chon, G., & Böhringer, H., 2012, A&A, 538, 35  
 Chon, G., & Böhringer, H., 2013, MNRAS, 429, 3272  
 Collins, C.A., Burke, D.J., Romer, A.K., et al., 1997, ApJ, 479, L117  
 Collins, C.A., Guzzo, L., Böhringer, H., et al., 2000, MNRAS, 319, 939  
 Croston, J.H., Pratt, G.W., Böhringer, H., et al., 2008, A&A, 487, 431  
 Daley, D.J., & Vere-Jones, D., 1988, An Introduction to the Theory of Point Processes, Springer, New York  
 de Grandi, S., Böhringer, H., Guzzo, L., et al., 1999, ApJ, 514, 148  
 Dikey, J.M. & Lockman, F.J., 1990, ARA&A, 28, 215  
 Donahue, M., Mack, J., Scharf, C., et al., 2001, ApJ, 552, L93  
 Dunkley, J., Spergel, D.N., Komatsu, E., et al., 2009, ApJS, 180, 306  
 Ebeling, H., Edge, A.C., Fabian, A.C., et al., 1997, ApJ, 479, 101  
 Edge, A.C., Stewart, G.C., Fabian, A.C., et al., 1990, MNRAS, 245, 559  
 Eisenstein, D.J. & Hu, W., 1998, ApJ, 496, 605

- Gioia, I.M., Maccacaro, T., Schild, R.E., et al., 1984, ApJ, 283, 495  
 Gioia, I.M., Henry, J.P., Mullis, C.R., et al., 2001, ApJ, 553, L105  
 Guzzo, L., Schuecker, P., Böhringer, H., et al., 2009, 499, 357  
 Hasselfield, M., Hilton, M., Marriage, T.A., et al., 2013, JACP, 7, 8  
 Henry, J.P., Gioia, I.M., Maccacaro, T., et al., 1992, ApJ, 386, 408  
 Henry, J.P., 2004, ApJ, 609, 603  
 Henry, J.P., Evrard, A.E., Hoekstra, H., et al., 2009, ApJ, 691, 1307  
 Hinshaw, G., Larson, D., Komatsu, E., et al., 2013, ApJS, 208, 19  
 Horner, D. J. 2001, PhD thesis, Univ. Maryland  
 Hu, W. & Kravtsov, A.V., 2003, ApJ, 584, 702  
 Ikebe, Y., Reiprich, T. H., Böhringer, et al., 2002, A&A, 383, 773  
 Kerscher, M., Mecke, K., Schuecker, P., et al., 2001, A&A, 377, 1  
 Kettula, K., Nevalainen, J., Miller, E.D., 2013, A&A, 552, A47  
 Koens, L.A., Maughan, B.J., Jones, L.R., et al. 2013, MNRAS, 435, 3231  
 Koester, B.P., McKay, T.A., Annis, J., et al. 2007a, ApJ, 660, 239  
 Komatsu, E., Smith, K.M., Dunkley, J., et al., 2011, ApJS, 192, 18  
 Kowalski, M.P., Ulmer, M.P., Cruddace, R.G., et al., 1984, ApJS, 56, 403  
 Ledlow, M.J., Loken, C., Burns, J.O., 1999, ApJ, 516, L53  
 Mahdavi, A., Hoekstra, H., Babul, A., et al., 2013, ApJ, 767, 116  
 Mantz, A., Allen, S.W., Ebeling, H., et al., 2008, MNRAS, 387, 1179  
 Marriage, T.B., Acquaviva, V., Ade, P.A.R., et al., 2011, ApJ, 737 61  
 Maughan, B., 2007, ApJ, 668, 772  
 Marshall, H.L., Avni, Y., Tannanbaum, H., Zamorani, G., 1983, ApJ, 269, 35  
 bibitem[Melin (2011)] Melin, J.-B., Bartlett, J.G., Delabrouille, J., et al., 2011, A&A, 525, A139  
 Meneghetti, M.; Rasia, E.; Merten, J., et al., 2010, A&A, 514, A93  
 Mullis, C.R., Vikhlinin, A., Henry, J.P., et al., 2004, ApJ, 607, 175  
 Nagai, D., Vikhlinin, A., Kravtsov, A.V., 2007, ApJ, 655, 98  
 Navarro, J., Frenk, C.S., White, S.D.M., 1995, MNRAS, 275, 56  
 Navarro, J., Frenk, C.S., White, S.D.M., 1997, ApJ, 490, 493  
 Nichol, R.C., Romer, A.K., Holden, B.P., et al., 1999, ApJ, 521, L21  
 Okabe, N., Zhang, Y.-Y., Finoguenov, A., et al., 2010, ApJ, 721, 8750  
 Ortiz-Gil, A., Guzzo, L., Schuecker, P., et al., 2004, MNRAS, 348, 325  
 PLANCK Collaboration, Ade, P.A.R., Aghanim, N., et al., 2013a, Planck results XX, A&A, submitted, arXiv1303.5080  
 PLANCK Collaboration, Ade, P.A.R., Aghanim, N., et al., 2013b, Planck results XVI, A&A, submitted, arXiv1303.5076  
 Pratt, G.W., Croston, J. H.; Arnaud, M., et al., 2009, A&A, 498, 361  
 Pratt, G.W., Arnaud, M., Piffaretti, R., et al., 2010, A&A, 511A, 85  
 Piccinotti, G., Mushotzky, R.F., Boldt, E.A., et al., 1982, ApJ, 253, 485  
 Reichardt, C.L., Stadler, B., Bleem, C.E., et al., 2013, ApJ, 763, 127  
 Reichert, A., Bhringer, H., Fassbender, R., Mhlegger, M., 2011, A&A, 535, A4  
 Reiprich T.H. & Böhringer, H., 2002, ApJ, 567, 716  
 Rosati, P., Della Ceca, R., Norman, C., et al., 1998, ApJ, 492, L21  
 Rosati, P., Borgani, S., Norman, C., 2002, ARA&A, 40, 539  
 Rozo, E., Wechsler, R.A., Rykoff, E.S., et al., 2010, ApJ, 708, 645  
 Sarazin, C.L., 1986, Rev. Mod. Phys., 58, 1  
 Schuecker, P. & Böhringer, H., 1998, A&A, 339, 315  
 Schuecker, P., Böhringer, H., Guzzo, L., et al., 2001, A&A, 368, 86  
 Schuecker, P., Guzzo, L., Collins, C.A., et al., 2002, MNRAS, 335, 807  
 Schuecker, P., Böhringer, H., Collins, C.A. et al., 2003a, A&A, 398, 867  
 Schuecker, P., Caldwell, R.R., Böhringer, H., et al., 2003b, A&A, 402, 53  
 Sehgal, N., Trac, H., Acquaviva, V., et al., 2011, ApJ, 732, 44  
 Spergel, D.N., Verde, L., Peiris, H.V., et al., 2003, ApJS, 148, 1755  
 Tinker, J., Kravtsov, A.V., Klypin, a., et al., 2008, ApJ, 688, 709  
 Tinker, J.L., Robertson, B.E., Kravtsov, A.V., et al., 2010, ApJ, 724, 878  
 Valdarnini, R. & Piffaretti, R., 2010, AIPC, 1248, 304  
 Vikhlinin, A., McNamara, B.R., Forman, W. et al., 1998, 498, L21  
 Vikhlinin, A., Kravtsov, A.V., Burenin, R.A., et al., 2009, ApJ, 692, 1060  
 Voevodkin, A. & Vikhlinin, A., 2004, ApJ, 601, 610  
 Voit, M., 2005, Rev. Mod. Phys., 77, 207  
 Voges, W., Aschenbach, B., Boller, T., et al. 1999, A&A, 349, 389  
 Trümper, J., 1993, Science, 260, 1769  
 Zhang, Y.-Y., Okabe, N., Finoguenov, A., et al., 2010, ApJ, 711, 1033

## Appendix A: Expected evolution of the X-ray luminosity function

Since we could not detect a significant evolutionary effect of the luminosity function as a function of redshift in the REFLEX II sample in our analysis in this paper, we take a closer look at the expected evolution. The evolution is driven by the building up the mass of clusters increasing the high mass end of the cluster mass function with time. But this evolutionary effect is partly

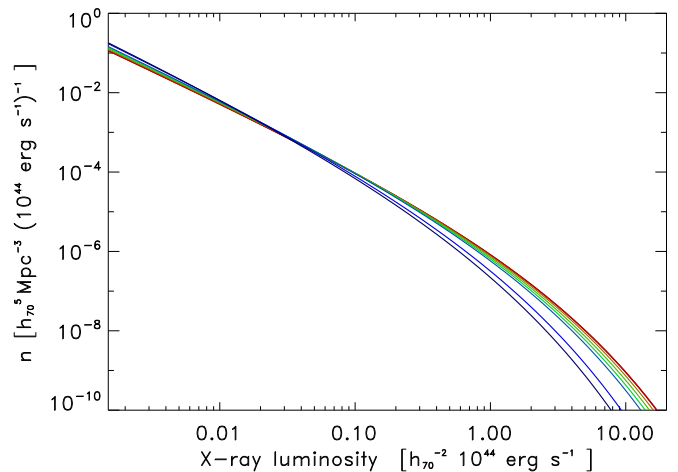


**Fig. A.1.** Predicted evolution of the X-ray luminosity function of galaxy clusters. The curves from top to bottom show the XLF for  $z = 0, 0.1, 0.2, 0.3, 0.4, 0.8, 1.0$ , respectively.

counteracted by the evolution of the  $L_X - M$  relation, so that the X-ray luminosity function shows very little evolution at low redshifts. This is illustrated in Fig. A.1 which shows the predicted X-ray luminosity function at redshifts from  $z = 0$  to 0.4 and at  $z = 0.8$  and 1. We note that unless we can probe the high mass end of the X-ray luminosity function very precisely at low redshift, we cannot not probe for this small effect. Due to the small volume of the survey at low redshifts we do not have the statistics to probe the high mass end sufficiently and thus we have no good leverage to constrain the luminosity function evolution. This does not imply, however, that there is no evolution of the cluster mass function.

## Appendix B: Shape dependence of the XLF on various parameters

In this section we show how the XLF depends on the cosmological parameters  $\Omega_m$  and  $\sigma_8$  on the one hand and on the slope and normalization parameter of the  $L_X - M$  scaling relation on the other hand to explain the behaviour of the parameter constraints in section 5. Fig. B.1 gives in the upper panel the effect of the cosmological parameters and in the lower panel the effect of the scaling relation parameters. We can see that e.g. an increase of the slope of the scaling relation makes the XLF steeper, which can be compensated by a larger  $\sigma_8$  counteracted by a smaller  $\Omega_m$  to keep the amplitude of the XLF in match.

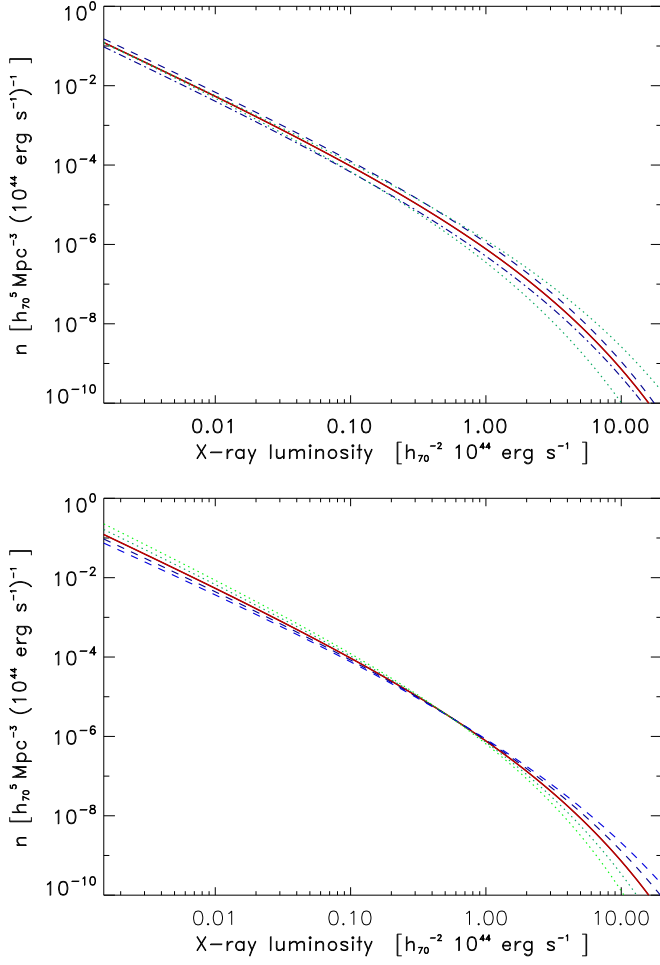


**Fig. B.1. Upper panel:** Variations of the predicted XLF with the change in the parameters  $\Omega_m$  and  $\sigma_8$ . The reference model (solid red line) has  $\Omega_m = 0.26$  and  $\sigma_8 = 0.8$ , the dashed line has  $\Omega_m = 0.30$  and the dot-dashed line  $\Omega_m = 0.22$ , while the upper dotted line shows the result for  $\sigma_8 = 0.9$  and the lower one for  $\sigma_8 = 0.7$ . **Lower panel:** Variations of the predicted XLF with the change in the parameter,  $\alpha_{sl}$  of the  $L_X - M$  scaling relation. The reference model (solid red line) has  $\alpha_{sl} = 1.51$ , the two dashed lines correspond to  $\alpha_{sl} = 1.61$  and  $1.71$  and the two dotted lines to  $\alpha_{sl} = 1.41$  and  $1.31$ .

